Flow Turbulence Combust (2016) 97:1147–1164
DOI 10.1007/s10494-016-9756-z

Evaluations of SGS Combustion, Scalar Flux and Stress Models in a Turbulent Jet Premixed Flame

K. Hiraoka[1] · Y. Naka[1] · M. Shimura[1] · Y. Minamoto[1] · N. Fukushima[2] · M. Tanahashi[1] · T. Miyauchi[3]

Received: 15 January 2016 / Accepted: 29 July 2016 / Published online: 11 August 2016
© Springer Science+Business Media Dordrecht 2016

Abstract A newly developed fractal dynamic SGS (FDSGS) combustion model and a scale self-recognition mixed (SSRM) SGS stress model are evaluated along with other SGS combustion, scalar flux and stress models in *a priori* and *a posteriori* manners using DNS data of a hydrogen-air turbulent plane jet premixed flame. *A posteriori* tests reveal that the LES using the FDSGS combustion model can predict the combustion field well in terms of mean temperature distributions and peak positions in the transverse distributions of filtered reaction progress variable fluctuations. *A priori* and *a posteriori* tests of the scalar flux models show that a model proposed by Clark et al. accurately predicts the counter-gradient transport as well as the gradient diffusion, and introduction of the model of Clark et al. into the LES yields slightly better predictions of the filtered progress variable fluctuations than that of a gradient diffusion model. Evaluations of the stress models reveal that the LES with the SSRM model predicts the velocity fluctuations well compared to that with the Smagorinsky model.

Keywords Large eddy simulation · SGS combustion model · SGS scalar flux model · SGS stress model · Turbulent jet premixed flame

✉ K. Hiraoka
khiraoka@navier.mes.titech.ac.jp

[1] Department of Mechanical and Aerospace Engineering, Tokyo Institute of Technology, 2-12-1 Ookayama, Meguro-ku, Tokyo, Japan

[2] Department of Mechanical Engineering, Tokyo University of Science, 6-3-1, Niijuku, Katsushika-ku, Tokyo, Japan

[3] Organization for the Strategic Coordination of Research and Intellectual Properties, Meiji University, 1-1-1 Higashimita, Tama-ku, Kanagawa, Japan

1 Introduction

Large eddy simulation (LES) of turbulent combustion is a promising tool for development of practical combustors because of recent increase of computational speed. In LES, physical quantities are separated into gird scale (GS) and subgrid scale (SGS) quantities by spatial filtering operation. The GS quantities are directly solved while contributions of SGS to GS phenomena are taken into account by mathematical models. For simulations of practical combustors such as gas turbine combustors and internal combustion engines, there are many modeling challenges such as modeling for flame propagation speed and heat release rate, reactants mixing, reaction mechanism, heat losses on the wall, local extinction and blow off, thermo-acoustic instabilities, formulation of pollutants such as NOx and soot, spark ignition, auto-ignition which induces knocking, liquid fuel vaporization, droplet combustion and radiative heat transfer. Although several attempts have been made to apply LES on existing gas turbines and engines [17], it is necessary to enhance performance of SGS models for the development of combustion devices.

Several approaches have been proposed to consider SGS combustion phenomena [19, 36, 46]. Filtered reaction rate and flame propagation speed are major targets for the combustion modeling; alternative approaches include probability density function and conditional moment closures [24, 43]. G-equation describes the propagation of flame surfaces assumed as infinitely thin scalar iso-surfaces [23, 33, 35]. To close the filtered G-equation, the turbulent burning velocity S_T needs to be predicted by an SGS combustion model. A reaction progress variable c is used as a representative of reactive scalars such as temperature or species mass fractions. In the filtered transport equation of the progress variable, a combustion model is required to calculate the flame surface density $\Sigma = \overline{|\nabla c|}$ [3], where $\bar{q}$ is a filtered quantity of q. Here, the flame surface density can be described using a winkling factor Ξ as $\Sigma = \Xi \times |\nabla \bar{c}|$ [5]. By applying the flamelet assumption [10], S_T is expressed using the ratio of flame surface areas of turbulent and laminar flames A_T/A_L, and Ξ is also computed with the flame surface areas [6] as:

$$S_T \sim \frac{A_T}{A_L} S_L \sim \Xi S_L, \tag{1}$$

where S_L denotes the laminar burning velocity. Therefore, modeling of the turbulent burning velocity, the flame surface density and the wrinkling factor has an equivalent meaning.

A number of combustion models have been proposed for the turbulent burning velocity [12, 35, 37, 48], the flame surface density [3, 25] and the wrinkling factor [5–7, 9, 14]. Pitsch and Duchamp De Lageneste [37] and Pitsch [35] developed models based on the transport equations of SGS scalar variance and flame brush thickness, respectively. Flohr and Pitsch [12] introduced a model based on the dimensional argument. Many models are based on fractal characteristics [5–7, 14, 25, 48]. In our previous study [20, 48], a fractal dynamic SGS (FDSGS) combustion model has been developed for the turbulent burning velocity, which is applicable to planar propagating premixed flames in homogeneous turbulence and turbulent jet premixed flames.

A scalar flux term, which is described as $f_i = \widetilde{u_i c} - \tilde{u}_i \tilde{c}$ in the transport equation of the progress variable, also requires a closure. Characteristics of the scalar flux in turbulent flames have been investigated [3, 11, 28] and many models were proposed [8, 21, 39, 44, 47]. Although a classical gradient diffusion hypothesis is generally employed as a first choice for modeling, counter-gradient transport phenomena have been observed [3, 15, 34]. Some models were developed to consider the counter-gradient transport [39, 44, 47]. Furthermore, the gradient diffusion model assumes the alignment of the scalar flux and

the scalar gradient. Huai et al. [21] proposed a model allowing for the anisotropy. *A priori* model evaluations have been performed using experimental data of turbulent V-shape flames by Pfadler et al. [34] and using DNS data of planar flames conducted with a single-step chemical reaction mechanism by Gao et al. [15].

An SGS stress model is also necessary to close the filtered momentum conservation equation. Although the Smagorinsky model is typically used, many models have been developed to adequately consider GS-SGS transfer of kinetic energy and complex flow geometry such as wall turbulence or free shear turbulent flows [1, 13, 16, 26, 32]. In a previous study [13], a scale self-recognition mixed (SSRM) SGS stress model has been proposed. *A priori* and *a posteriori* tests show that the model has superiority for the accuracy against the Smagorinsky model in non-reactive homogeneous isotropic turbulence [13].

The SGS combustion, scalar flux and stress models interact with each other and affect overall predictability of the LES. For the development of the highly accurate models, it is necessary to clarify the accuracy and interactions of the complete set of the models in the LES of turbulent premixed flames. Therefore, in the present study, the FDSGS combustion model, scalar flux models and the SSRM stress model are evaluated. This work focuses on a reaction progress variable approach. *A priori* tests of several flux models are performed with DNS data of a hydrogen-air turbulent jet premixed flame considering a detailed kinetic mechanism and temperature dependence of the thermal and transport properties [41]. Then, the LES of the turbulent jet flame is performed using the FDSGS combustion model, the flux models and the SSRM model for *a posteriori* model evaluations. The present paper first describes the mathematical background of the FDSGS combustion model in Section 2 and the SSRM stress model in Section 3. Then, the methodology and conditions of the DNS are explained in Section 4. The *a priori* tests of the flux models are discussed in Section 5. Finally, the *a posteriori* tests of the SGS combustion, scalar flux and stress models are discussed in Section 6.

2 Fractal Dynamic SGS Combustion Model

In this section, the FDSGS combustion model, used to predict Ξ, is explained briefly. The detailed derivations are found in a literature [20, 48]. The model consists of two parts that represent effects of turbulence motion and dilatation of fluid due to heat release:

$$\frac{S_T}{S_L} \sim \frac{A_T}{A_L} \sim \frac{A_T}{\Delta^2} = \frac{A_{\mathrm{turb}}}{\Delta^2} + \frac{A_{\mathrm{dila}}}{\Delta^2}, \tag{2}$$

where A_{turb} and A_{dila} denote the contributions of the turbulence and dilatation effects on the flame surface area, respectively. Δ is the filter width of LES. The turbulence contribution A_{turb} is modeled based on the fractal characteristics of flame surfaces and a scale separation assumption in high Reynolds number turbulence as:

$$\frac{A_{\mathrm{turb}}}{\Delta^2} = \left(\frac{\alpha^4 \nu^3}{2\sqrt{2} C_s^2 \Delta^6}\right)^{(2-D_3)/4} \left\{\tilde{S}_{ij}\tilde{S}_{ij} - \mathrm{div}\,(\tilde{\boldsymbol{u}})^2\right\}^{-3(2-D_3)/8}, \tag{3}$$

where ν, C_s and S_{ij} represent the kinematic viscosity, the Smagorinsky coefficient and the strain rate tensor, and $\tilde{q}$ is a Farvre filtered quantity of any quantities q. D_3 denotes the fractal dimension of flame surfaces and is dynamically computed using a fractal dynamic SGS (FDSGS) model [20, 31]. The FDSGS model performs a box-counting method on the LES flame surfaces at a grid scale Δ and on test-filtered flame surfaces at a test-filter scale $\hat{\Delta}$ $(= 2\Delta)$ in control volumes (CVs). In this study, CVs of two different sizes, 4Δ and 8Δ

are employed. α is a scaling factor determined from a correlating equation for inner cutoff ϵ_{in} of flame surfaces [40] as:

$$\alpha = \frac{\epsilon_{in}}{\eta} \approx 8 \exp\left(6.0 \frac{\delta_F}{D}\right), \tag{4}$$

where η, δ_F and D are the Kolmogorov length scale, Zel'dovich flame thickness computed as ν/S_L and the most expected diameter of coherent fine scale eddies ($D \approx 8\eta$) [40, 42]. The Kolmogorov length scale is estimated using:

$$\eta \approx \left(\frac{\nu^3}{2\sqrt{2}(C_s\Delta)^2(\tilde{S}_{ij}\tilde{S}_{ij} - \mathrm{div}\,(\tilde{\boldsymbol{u}})^2)^{3/2}}\right)^{1/4}. \tag{5}$$

The dilatation contribution A_{dila} is a correction term to reproduce the laminar burning velocity and modeled based on the flamelet concept as:

$$\frac{A_{\mathrm{dila}}}{\Delta^2} = \frac{\delta_\Delta}{\delta_{th}} \frac{\mathrm{div}\,(\tilde{\boldsymbol{u}})}{(\mathrm{div}\,(\boldsymbol{u})_L)\big|_{F_0}}, \tag{6}$$

where δ_{th} is the thermal flame thickness and the subscript F_0 denotes a value which is used to identify flame surface defined based on G or c. δ_Δ represents a pseudo flame thickness of a filtered laminar flame expressed as:

$$\delta_\Delta = \int_{-\Delta/2}^{\Delta/2} \mathrm{div}\,(\tilde{\boldsymbol{u}})_L\, dx / \left(\mathrm{div}\,(\tilde{\boldsymbol{u}})_L\right)\big|_{\tilde{F}=F_0}. \tag{7}$$

3 Scale Self-Recognition Mixed SGS Stress Model

This section describes the SSRM stress model. Details of the model derivations are found in a literature [13]. The SSRM model is a mixed stress model which applies the Bardina model [1] for the cross term and a Smagorinsky-type model for the Reynolds term. The model describes the SGS stress tensor τ_{ij} as:

$$\tau_{ij} = \left(\overline{\bar{u}_i\bar{u}_j} - \bar{u}_i\bar{u}_j\right) + \left(\bar{\bar{u}}_i\left(\bar{u}_j - \bar{\bar{u}}_j\right) + \bar{\bar{u}}_j\left(\bar{u}_i - \bar{\bar{u}}_i\right)\right) - \left(2\left(C_{\mathrm{SSRM}}\Delta\right)^2|\bar{S}|\bar{S}_{ij}\right). \tag{8}$$

The model coefficient C_{SSRM} is dynamically determined using a correlating equation [13] with the ratio of the grid width to the Kolmogorov length scale Δ/η as:

$$C_{\mathrm{SSRM}} = C_\infty\left\{1 - a_1 \exp\left(-a_2\frac{\Delta}{\eta}\right)\right\}, \tag{9}$$

where C_∞, a_1 and a_2 are model constants of $C_\infty = 0.15$, $a_1 = 1.155$ and $a_2 = 0.04274$. The ratio of the grid width to the Kolmogorov length scale Δ/η is calculated with a relationship [13]:

$$\frac{\Delta}{\eta} = b_1\left(\frac{2\Delta^6|\bar{S}|\bar{S}_{ij}\bar{S}_{ij}}{\nu^3}\right)^{b_2} \tag{10}$$

Here, the model constants, b_1 and b_2 are 0.3328 and 0.2651, respectively. The SSRM model was originally proposed for non-reactive incompressible turbulence. It is confirmed for the high Reynolds number homogeneous isotropic turbulence that the model coefficient C_{SSRM} is a function of Δ/η and it can be expressed by the grid scale strain rate tensor [13]. The model constants are determined with DNS data of the homogeneous isotropic turbulence.

In this study, the model is extended to compressible turbulent combustion by replacing the filter operation $\bar{q}$ with Favre filter operation $\tilde{q}$ in Eqs. 8 and 10.

4 Direct Numerical Simulation of a Turbulent Jet Premixed Flame

A priori and *a posteriori* tests of the models are performed using the DNS data of a hydrogen-air turbulent plane jet premixed flame. In this section, the methodology and conditions of the DNS are summarized [41]. Fully-compressible governing equations for mass, momentum, energy and mass fractions of chemical species are solved. Soret effect, Dufour effect, pressure gradient diffusion, bulk viscosity and radiative heat transfer are assumed to be negligible. The hydorgen-air chemical reaction is considered using a detailed kinetic mechanism consisting of 12 reactive species (H_2, O_2, H_2O, O, H, OH, HO_2, $H_2O_2N_2$, N, NO_2 and NO) and 27 elementary reactions [18]. The temperature dependence of the viscosity, the thermal conductivity and the mass diffusion coefficients is taken into account. The governing equations are spatially discretized with a fourth order central finite difference scheme. To eliminate numerical oscillations in the higher frequency than spatial resolution of the finite difference scheme, a fourth order compact finite difference filter [27] is applied. Time integration is performed usinzg a third-order Runge-Kutta scheme. A point implicit method with VODE solver [4] is employed for chemical source terms since the use of the detailed chemistry causes a stiff problem.

Figure 1 shows the DNS configuration. A jet flow of unburned mixture and surrounding co-flow streams of burnt gas are issued at an inflow boundary. The inflow and non-reflecting outflow boundary conditions are applied in x and y directions based on Navier-Stokes characteristic boundary conditions (NSCBC) [2, 38], and a periodic boundary condition is

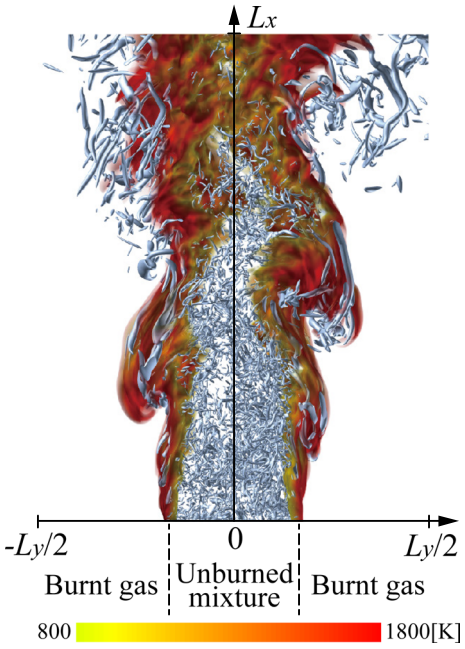

Fig. 1 DNS configuration and simulated jet flame. Temperature distribution visualized by the volume rendering method and contour surfaces of the second invariant of velocity gradient tensor $Q/Q_{\max} = 0.018$

employed in z direction. The computational domain size is $L_x \times L_y \times L_z = 20 \times 16 \times 8\text{mm}^3$ and the number of grid points is $N_x \times N_y \times N_z = 1281 \times 1025 \times 513$, which ensures 30 grid points within the thermal flame thickness δ_{th}. The mean inflow velocity distribution $U(y)$ is given by combining two hyperbolic tangent velocity profiles with the the vorticity thickness $\delta_{\omega,0} = \left(u_{jet} - u_{cof}\right) / \left(\partial U/\partial y\right)_{\max}$ of 0.5mm, where u_{jet} and u_{cof} are the mean inflow velocities of the unburned mixture ($u_{jet} = 350$m/s) and the burnt gas ($u_{cof} = 20$m/s), respectively. The jet width is set to 5.0mm and the mosts unstable wave length of the velocity distribution is $\Lambda = 7.066\delta_{\omega,0}$ [30]. Mean flow-through time of the present configuration, which is calculated as mean jet convection time from the inflow to outflow boundaries, is $\tau_{ft} = 57\mu$s. The simulation was run for $1.2\tau_{ft}$ from a initial condition until initial transients left. Then, the computation was continued for additional $0.9\tau_{ft}$ and 6 snapshots are collected for the analysis.

Equivalence ratio, temperature and pressure of the unburned mixture are set to be 1.0, 700K and 0.1MPa, respectively. Fully developed homogeneous isotropic turbulence obtained by a preliminary incompressible DNS is superimposed on the mean inflow velocity of the unburnt mixture as velocity fluctuations. Table 1 presents the inflow turbulence characteristics. Re_λ and Re_l represent the Reynolds numbers based on the Taylor micro-scale λ and the integral length scale l. η_{in}, u', Da and Ka denote the Kolmogorov length scale, turbulent intensity, the Damköhler number $Da = (l/\delta_F) / \left(u'/S_L\right)$ and the Karlovitz number $Ka = \left(u'/S_L\right)^{3/2} (l/\delta_F)^{-1/2}$, respectively. The inflow turbulence condition locates near the boundary between the corrugated flamelets regime and the thin reaction zones regime in the turbulent combustion diagram of Peters [33] as shown in Fig. 2 with a red symbol. In Fig. 2, local turbulent characteristics along the streamwise direction in the unburned region are also plotted with blue symbols. The unburned region is defined based on temperature as the region with $T < T_{HRR}$, where T_{HRR} (= 1282K in the present condition) is the temperature at which heat release rate shows the maximum in an unstrained laminar flame with the same unburned mixture as the DNS. In the upstream region, l increases in the streamwise direction, while the value obtained from the average of limited samples fluctuate because of the large scale roller structures driven by the Kelvin-Helmholtz (KH) instability in the downstream region.

The simulated flame is shown in Fig. 1 to clarify general flame features. The gray surfaces represent the contour surfaces of the second invariant of velocity gradient tensor, $Q/Q_{\max} = 0.018$ and temperature distribution is visualized by the volume rendering method. The large scale roller structures driven by the KH instability significantly wrinkle the flame, while vortices in the inflow turbulence and eddy structures generated by the turbulent transition in the shear flow generate fine scale flame wrinkling toward downstream.

5 *A Priori* Tests of the SGS Scalar Flux Models

In this section, the SGS scalar flux models are evaluated by *a priori* tests using the DNS data of the jet flame. For the analysis, the velocity and progress variable fields of the DNS

Table 1 Turbulent characteristics of the inflow unburned mixture

Re_λ	Re_l	u'[m/s]	l[mm]	λ[mm]	$\eta_{in}[\mu$m]	u'/S_L	l/δ_F	Da	Ka
97.1	516	40.0	1.17	0.161	11.5	3.87	133	34.6	0.655

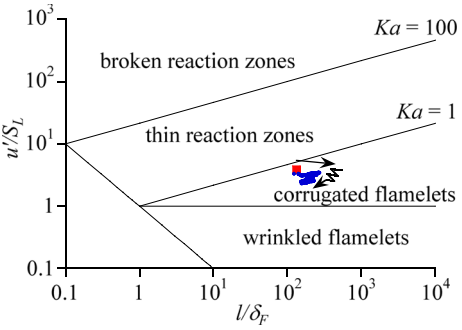

Fig. 2 Present DNS condition on a turbulent combustion diagram proposed by Peters [33]. Red symbol denotes the inflow turbulence characteristics. Blue symbol represents the local turbulent characteristics along the streamwise direction in the unburned region

data are filtered with the Gaussian filter in the density-weighted manner. The progress variable is defined based on temperature as $c = (T - T_u) / (T_b - T_u)$, where T_u and T_b denote temperature of the unburned mixture and burnt gas in the corresponding laminar flame. The filter width is taken to be $\Delta = 21.7\eta_{in}$ or $\Delta = 43.3\eta_{in}$. To reveal general characteristics of the scalar flux, contour surfaces of $\bar{\rho} f_i n_i$ of an instantaneous field obtained from the filtered DNS data for $\Delta = 21.7\eta_{in}$ are shown in Fig. 3, where f_i is the scalar flux $f_i = \widetilde{u_i c} - \tilde{u}_i \tilde{c}$ and n_i is a unit normal vector to progress variable iso-surfaces $n_i = \nabla\tilde{c}/|\nabla\tilde{c}|$. The blue and green surfaces represent the iso-surfaces with $\bar{\rho} f_i n_i / \rho_u S_L = -0.065$ and 0.065 respectively, where ρ_u is the unburned mixture density. Flame surfaces defined as temperature contour surfaces of $T = T_{HRR}$ and the contour surfaces of the second invariant of velocity gradient tensor $Q/Q_{max} = 0.025$ are also visualized as red and gray surfaces,

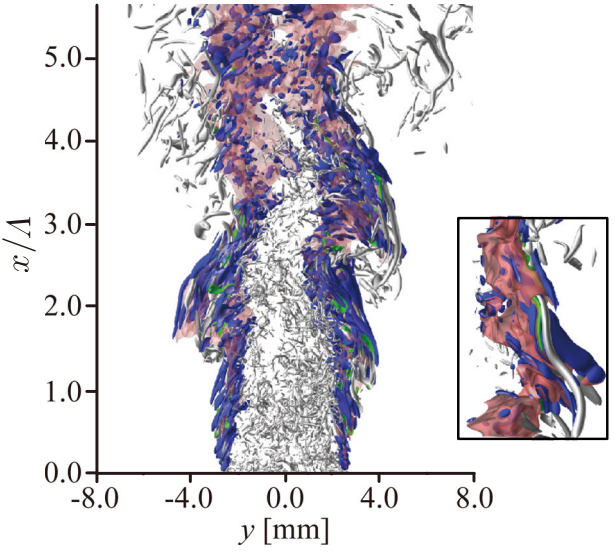

Fig. 3 Contour surfaces of the inner product of the SGS scalar flux and the unit normal vector to progress variable iso-surfaces (blue surfaces: $\bar{\rho} f_i n_i / \rho_u S_L = -0.065$, green surfaces: $\bar{\rho} f_i n_i / \rho_u S_L = 0.065$), contour surfaces of the second invariant of velocity gradient tensor $Q/Q_{\max} = 0.025$ (*gray surfaces*) and temperature contour surfaces of $T = 1282$K (*red surfaces*) for the filter width of $\Delta = 21.7\eta_{in}$ for the entire flame and at a near field region with the counter-gradient transport (*in-set figure*)

respectively. $f_i n_i < 0$ and $f_i n_i > 0$ represent the gradient diffusion and counter-gradient transport, respectively. The intensive scalar transport is observed near the flame surfaces and the shear layer especially close to the large scale roller structures. A near field region with the counter-gradient transport is also visualized in Fig. 3. Between the flame surface and a long streamwise eddy, a region with the counter-gradient transport exists along with the eddy structure. A previous study showed that the occurrence of the counter-gradient transport is characterized with the normalized turbulence intensity u'/S_L in the RANS context [45]. The counter-gradient transport is observed for the present jet flame with the inflow turbulence intensity of $u'/S_L = 3.87$. Previous studies also reported the counter-gradient transport in planar flames in homogeneous turbulence for $u'/S_L = 7.5$ [15] and 4.0 [3] and in V-shape flames for $u'/S_L = 0.37$ and 2.0 [34] and for $1.25 \leq u'/S_L \leq 3.75$ [11].

For *a priori* model evaluations, the flux is calculated by the models using the filtered DNS data. The model predictions are compared with the values directly calculated from the DNS data. The samples are taken from the whole computational domain of an instantaneous field at the time instant in Fig. 3. Several models summarized in the Table 2 are tested. In a previous study by Gao et al. [15], the models proposed by Clark et al. [8] and Huai et al. [21] showed superiority for the accuracy than other several conventional models. Eddy viscosity ν_t needed in the gradient diffusion model and the model of Huai et al. [21] is calculated with the Smagorinsky model. The Smagorinsky coefficient C_s, turbulent Schmidt number Sc_t and a model constant D_{an} in the model of Huai et al. [21] are set to be $C_s = 0.16$, $Sc_t = 0.7$ and $D_{an} = 0.14$, respectively. Figure 4 shows joint probability density functions of $\bar{\rho} f_i n_i$ predicted by the models ($\bar{\rho} f_{i:\mathrm{model}} n_i$) and obtained from the DNS data ($\bar{\rho} f_{i:\mathrm{DNS}} n_i$). The gradient diffusion model predicts the gradient transport only, and the magnitude of the gradient transport tends to be larger than the DNS data. The model of Huai et al. [21] consists of the gradient diffusion term and an additional term to represent the anisotropy. The anisotropic term can predict the counter-gradient transport while the model overestimates the magnitude of the gradient transport under the present conditions. This is because the gradient transport is considered by both the gradient diffusion and anisotropic terms (not shown). Pfadler et al. [34] also discussed that the use of only the anisotropic term improves the model accuracy. The model of Clark et al. [8] predicts the counter-gradient transport as well as the gradient transport, and shows good correlations with the DNS data. Figure 5 shows a JPDF of $\bar{\rho} f_{i:\mathrm{DNS}} n_i$ and angle Θ between $\bar{\rho} f_{i:\mathrm{DNS}}$ and n_i for the filter width of $\Delta = 21.7\eta_{in}$. The SGS scalar flux is not aligned with the gradient of the progress variable in the most computational domain. This causes worsened predictions by the gradient diffusion model. The model of Clark et al. [8] orients the scalar flux by taking account of velocity gradient, which is one of the reasons for the good predictability of the counter-gradient transport.

Table 2 SGS scalar flux models considered in the *a priori* and *a posteriori* tests

	Expressions for the SGS scalar flux
Gradient diffusion model	$f_i = -\dfrac{\nu_t}{Sc_t}\dfrac{\partial \tilde{c}}{\partial x_i}$
Clark et al. [8]	$f_i = \dfrac{\Delta^2}{12}\dfrac{\partial \tilde{u}_i}{\partial x_k}\dfrac{\partial \tilde{c}}{\partial x_k}$
Huai et al. [21]	$f_i = -\dfrac{\nu_t}{Sc_t}\dfrac{\partial \tilde{c}}{\partial x_i} + D_{an}\Delta^2 \tilde{S}_{ik}\dfrac{\partial \tilde{c}}{\partial x_k}$

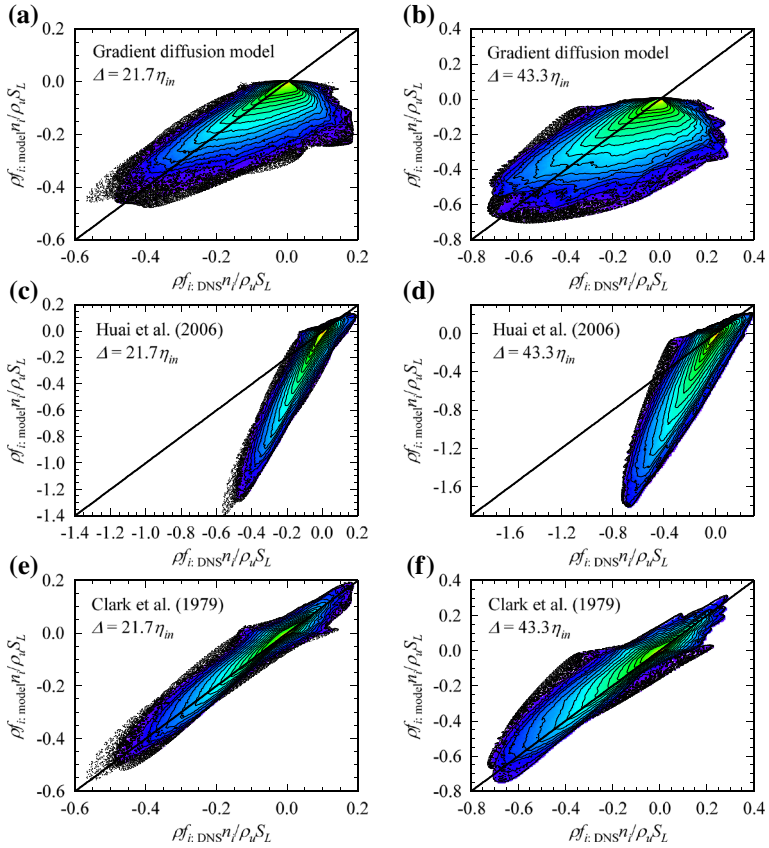

Fig. 4 JPDFs of $\bar{\rho} f_i n_i$ predicted by the gradient diffusion model (**a**, **b**) and the models of Huai et al. [21] (**c**, **d**) and Clark et al. [8] (**e**, **f**), and obtained from the DNS data for the filter width of $\Delta = 21.7\eta_{in}$ (**a**, **c**, **e**) and $\Delta = 43.3\eta_{in}$ (**b**, **d**, **f**). Black line indicates the perfect agreement

6 *A Posteriori* Tests of SGS Combustion, Scalar Flux and Stress Models

6.1 LES of the turbulent jet premixed flame

LES of the jet flame in the identical configuration and condition to the DNS is performed for *a posteriori* assessments of the FDSGS combustion model, the scalar flux models and the SSRM stress model. The LES solves following filtered conservation equations for mass:

$$\frac{\partial \bar{\rho}}{\partial t} + \frac{\partial \left(\bar{\rho}\tilde{u}_i\right)}{\partial x_i} = 0, \tag{11}$$

and momentum:

$$\frac{\partial \left(\bar{\rho}\tilde{u}_i\right)}{\partial t} + \frac{\partial \left(\bar{\rho}\tilde{u}_i\tilde{u}_j\right)}{\partial x_j} = -\frac{\partial \bar{p}}{\partial x_i} + \frac{\partial}{\partial x_j}\left(-\frac{2}{3}\mu\frac{\partial \tilde{u}_k}{\partial x_k}\delta_{ij} + \mu\left(\frac{\partial \tilde{u}_i}{\partial x_j} + \frac{\partial \tilde{u}_j}{\partial x_i}\right)\right) - \frac{\partial \left(\bar{\rho}\tau_{ij}\right)}{\partial x_j}, \tag{12}$$

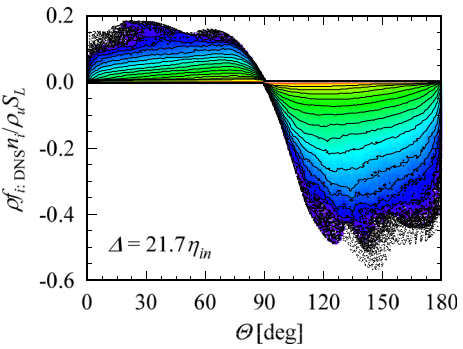

Fig. 5 JPDF of $\bar{\rho} f_i n_i$ and angle Θ between the SGS scalar flux $\bar{\rho} f_i$ and the unit normal vector to progress variable iso-surfaces n_i which are obtained from the DNS data for the filter width of $\Delta = 21.7\eta_{in}$

and a transport equation of the reaction progress variable based on temperature:

$$\bar{\rho}\frac{\partial \tilde{c}}{\partial t} + \bar{\rho}\tilde{u}_i \frac{\partial \tilde{c}}{\partial x_i} = \rho_u \Xi S_L |\nabla \tilde{c}| - \frac{\partial \left(\bar{\rho} f_i\right)}{\partial x_i}. \tag{13}$$

The pressure is calculated using the equation of state for ideal gas. Mass fractions of chemical species are binarized as $\tilde{Y}_i = Y_{i,u}(\tilde{c} < c_0)$ and $Y_{i,b}(\tilde{c} \geq c_0)$, where c_0 is a value of c corresponding to the temperature $T = T_{HRR}$ and the subscripts u and b denote quantities in unburned and burnt gas of the corresponding unstrained laminar flame, respectively. The equations are spatially discretized using a fourth-order central finite difference scheme. For the discretization of the convection term in the transport equation of c, a fifth-order weighted essentially non-oscillatory (WENO) scheme [22, 29] is applied. To eliminate numerical oscillations in higher frequency than spatial resolution of the finite difference scheme, a fourth-order compact finite difference filter [27] is used. Time integration is performed with a third-order Runge-Kutta scheme.

For the inflow turbulence, the same homogeneous isotropic turbulence as that in the DNS is filtered with the Gaussian and cutoff filters, and superimposed on the mean inflow velocity. In the streamwise (x) and transverse (y) directions, a convective outflow boundary condition is applied for the transport equation of c, and the inflow and outflow boundary conditions using the NSCBC formulation [2, 38] are employed for the other equations. A periodic boundary condition is set in the spanwise (z) direction. The grid sizes Δ, the computational domain sizes $L_x \times L_y \times L_z$ and the number of grid points $N_x \times N_y \times N_z$ of the DNS and the LES are summarized in Table 3. The LES computation was conducted for $0.9\tau_{ft}$-$3.2\tau_{ft}$ after initial flow field transients left and 130-300 snapshots are collected for averaging in the following model evaluations.

Table 3 Configuration parameters of the LES and the DNS

	Δ/η_{in}	L_x[mm] $\times$ L_y[mm] $\times$ L_z[mm]	$N_x \times N_y \times N_z$
DNS	1.36	$20 \times 16 \times 8$	$1281 \times 1025 \times 513$
LES11	10.8		$321 \times 385 \times 65$
LES22	21.7	$40 \times 48 \times 8$	$161 \times 193 \times 33$
LES43	43.3		$81 \times 97 \times 17$

Table 4 SGS combustion models considered in *a posteriori* tests

	Expressions for the wrinkling factor
Pitsch and Duchamp De Lageneste [37]	$\Xi = 1 + \frac{u'_\Delta b_3}{S_L}\left[\left(\frac{Da_\Delta}{Sc_\Delta}\right) / \left(1 + \frac{b_3^2 Da_\Delta}{b_1^2 Sc_\Delta}\right)\right]^{1/2}$, $b_1 = 2.0, b_3 = 1.0$
Chatakonda et al. [7]	$\Xi = \left(1 + \frac{\Delta}{\epsilon_{in}}\right)^\beta$, $\beta = 1/3 + 1/3\,(\eta_{oc}/b)^x \,/\, \left((L_G/a)^x + (\eta_{oc}/b)^x\right)$, $\epsilon_{in} = \left((L_G/a)^x + (\eta_{oc}/b)^x\right)^{1/x}$, $a = 2.0, b = 0.145, x = 4.0$

The SSRM stress model and the Smagorinsky model are used to compute the SGS stress tensor τ_{ij}. The Smagorinsky coefficient is set to $C_s = 0.16$. The models in Table 2 are employed for the SGS scalar flux model. The turbulent Schmidt number Sc_t and a model constant D_{an} in the model of Huai et al. [21] are set to be $Sc_t = 0.7$ and $D_{an} = 0.14$, respectively. The FDSGS combustion model and two conventional combustion models summarized in Table 4 are applied to obtain the flame wrinkling factor Ξ. A Smagorinsky-type model [12] is used to estimate the SGS turbulent velocity fluctuation in the conventional models [7, 37] as $u'_\Delta = C_s \Delta |\tilde{S}_{ij}|$.

Figure 6 shows the instantaneous flame surfaces defined as temperature contour surfaces of $T = T_{HRR}$ and temperature distributions on an x-y plane obtained from the LES using the FDSGS combustion model with the CV of size 4Δ, the gradient diffusion model and the Smagorinsky model. For comparison, a distribution at the same time instant in the DNS is also visualized. It is found that small scale wrinkling of the flame surfaces is not resolved in the LES. As for the flame shape at large scale such as the flame wrinkling due to the large scale roller structures, the LES result agrees qualitatively well with the DNS data.

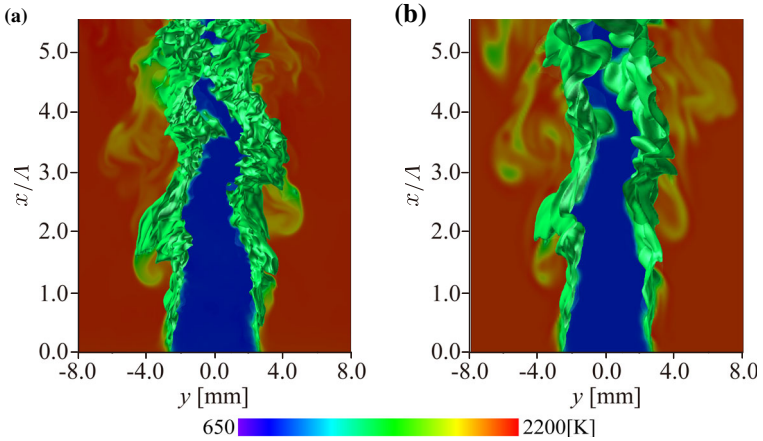

Fig. 6 Instantaneous flame surfaces and temperature distributions on an x-y plane for the DNS (**a**) and for LES11 (**b**) using the FDSGS combustion model with the CV of size 4Δ, the gradient diffusion model and the Smagorinsky model

6.2 Evaluations of the SGS combustion models

To evaluate influences of the SGS combustion models, the stress and scalar flux models are fixed to the Smagorinsky model and the gradient diffusion model in this section. Figure 7 shows transverse distributions of mean temperature at $x/\Lambda = 2.0$ and 4.0 for the LES and for the DNS data filtered with the Gaussian and cutoff filters. Results based on the FDSGS combustion model and the models in Table 4 are shown. The temperature distributions of the LES using the FDSGS combustion model show reasonable agreement with the DNS data almost being independent of the grid width and the streamwise position although the LES with the CV of size 8Δ gives slightly higher values than the DNS. The results with the model of Chatakonda et al. [7] also give relatively good predictions, but they slightly overestimate the temperature in the upstream region as the grid width increases. The LES using the model of Pitsch et al. [37] predicts higher values than the DNS under the present conditions. As discussed in our previous study [20], the Smagorinsky-type model [12] overestimates the

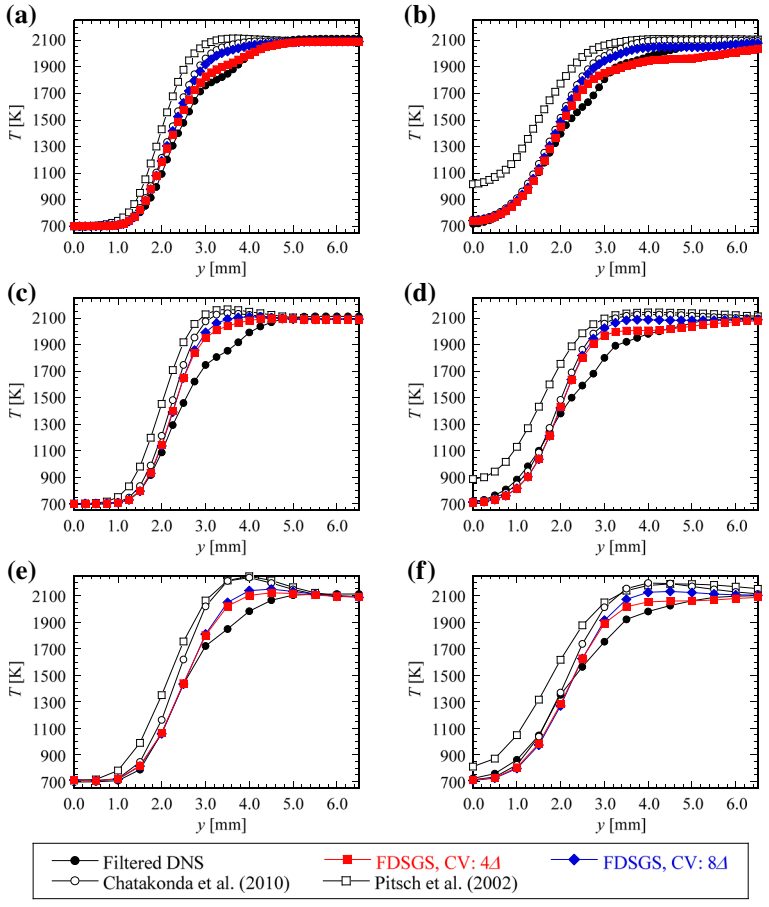

Fig. 7 Transverse distributions of mean temperature for the filtered DNS data and for LES11 (**a**, **b**), LES22 (**c**, **d**) and LES43 (**e**, **f**) at $x/\Lambda = 2.0$ (**a**, **c**, **e**) and 4.0 (**b**, **d**, **f**)

SGS turbulent velocity fluctuation, which may cause the overpredictions of the turbulent burning velocity and therefore, result in the higher temperature.

In Fig. 8, the transverse distributions for root-mean-square (RMS) fluctuation c'' of the filtered progress variable from the average values are shown. Compared with the mean temperature distributions in Fig. 7, the LES predictions of c'' show large deviations from the DNS data especially in LES11 and LES43 for all model cases. However, the LES using the FDSGS combustion model and the model of Chatakonda et al. [7] predicts peak positions of the c'' distributions and gives reasonable performance. The results with the model of Pitsch et al. [37] tend to show higher values than the DNS toward the downstream as the grid width decreases. From the results in Figs. 7 and 8, it is found that the FDSGS combustion model and the model of Chatakonda et al. [7] gives good predictions under the conditions of the present study. The good applicability of the FDSGS combustion model holds when it is used with the SSRM stress model and other scalar flux models. The performance of such combination is demonstrated in the later section.

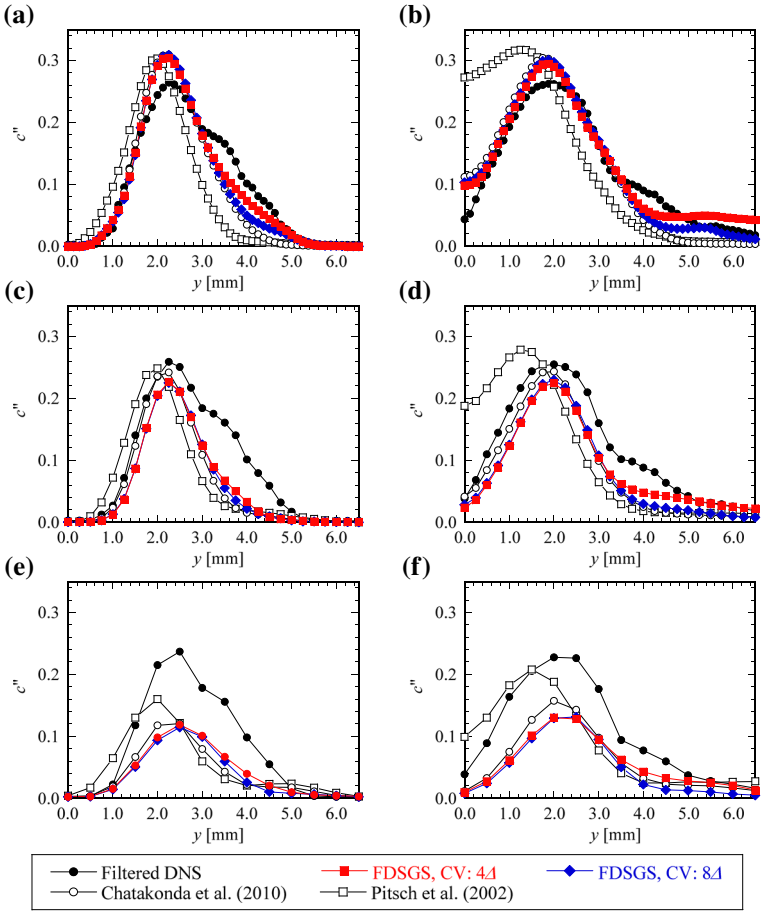

Fig. 8 Transverse distributions of c'' for the filtered DNS data and for LES11 (**a**, **b**), LES22 (**c**, **d**) and LES43 (**e**, **f**) at $x/\Lambda = 2.0$ (**a**, **c**, **e**) and 4.0 (**b**, **d**, **f**)

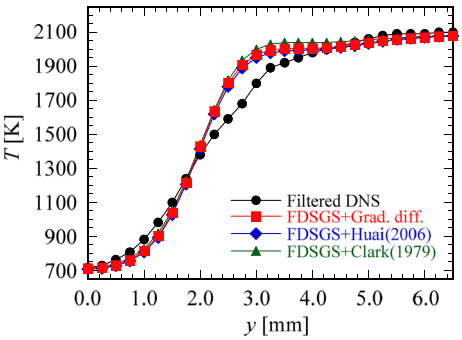

Fig. 9 Transverse distributions of mean temperature for the filtered DNS data and for LES22 at $x/\Lambda = 4.0$

6.3 Evaluations of the SGS scalar flux models

The effects of the SGS scalar flux models are evaluated in this section. Figure 9 shows the mean temperature distributions at $x/\Lambda = 4.0$ for the LES22 with the flux models summarized in Table 2 and for the filtered DNS data. The FDSGS combustion model with the CV of size 4Δ and the Smagorinsky model are applied for the combustion and stress models, respectively. It is found that the differences in the mean temperature distributions for different scalar flux models are not significant.

The c'' distributions of LES22 and LES43 are shown in Fig. 10. The LES with the model of Clark et al. [8] predicts slightly higher values and gives better predictions than that with the gradient diffusion model, while that with the model of Huai et al. [21] predicts slightly lower values under the present conditions. This trend of good predictability for the model of Clark et al. [8] is also seen when the combustion model of Chatakonda et al. [7] is employed (not shown). However, the LES results are more sensitive to the SGS combustion model rather than the scalar flux model. Boger et al. [3] also discussed that the contributions of the SGS scalar flux on the whole LES predictivity are not significant.

6.4 Evaluations of the SGS stress models

The assessment of the SSRM stress model is performed in this section. Figure 11 shows the transverse distributions of mean streamwise velocity U and mean transverse velocity V at $x/\Lambda = 4.0$ of the LES22 and the filtered DNS data. The FDSGS combustion model with the CV of size 4Δ, the model of Clark et al. [8] and the SSRM stress model or the

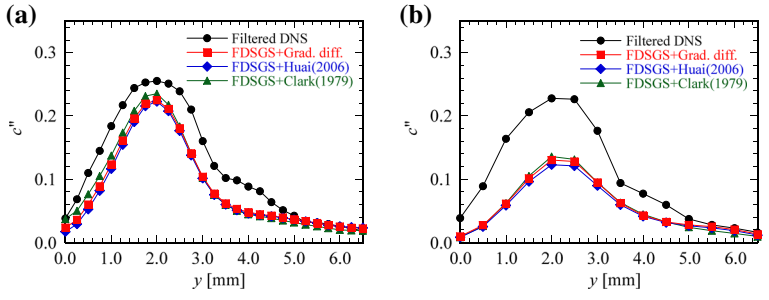

Fig. 10 Transverse distributions of c'' for the filtered DNS data and for LES22 (**a**) and LES43 (**b**) at $x/\Lambda = 4.0$

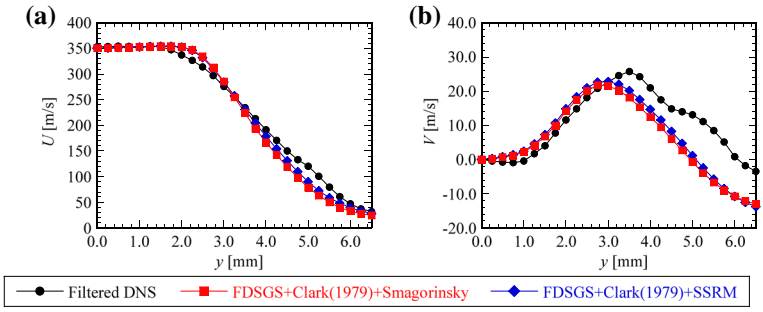

Fig. 11 Transverse distributions of U (**a**) and V (**b**) for the filtered DNS data and for LES22 at $x/\Lambda = 4.0$

Smagorinsky model are used as the combustion, scalar flux and stress models, respectively. Differences in the LES predictivities with the SSRM model and the Smagorinsky model are not significant.

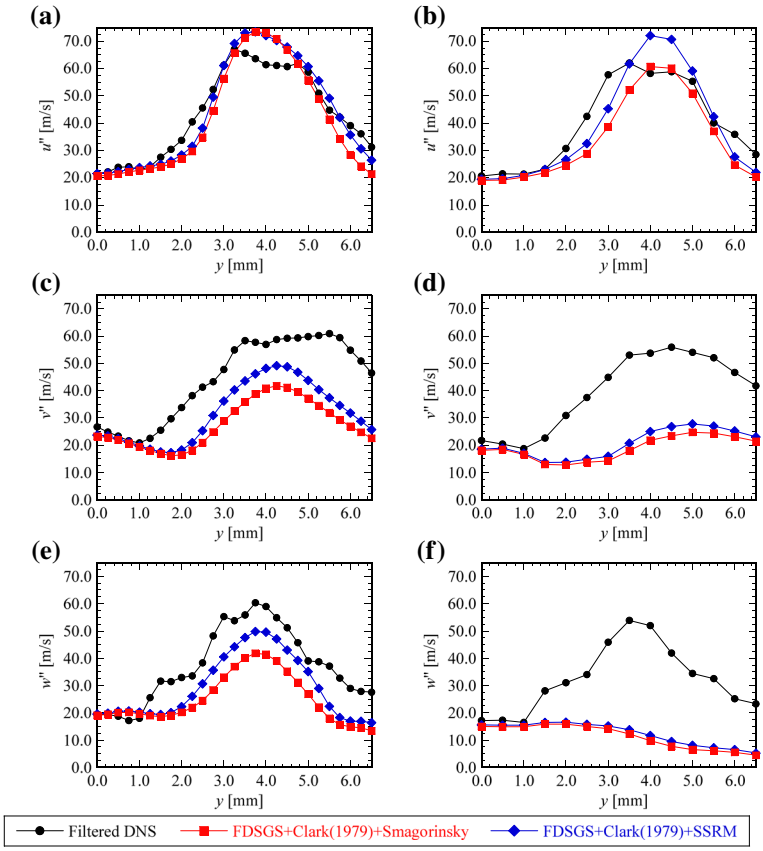

Fig. 12 Transverse distributions of u'' (**a**, **b**), v'' (**c**, **d**) and w'' (**e**, **f**) for the filtered DNS data and for LES22 (**a**, **c**, **e**) and LES43 (**b**, **d**, **f**) at $x/\Lambda = 4.0$.

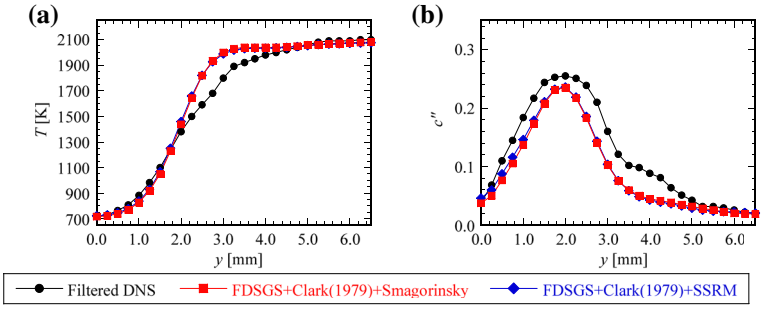

Fig. 13 Transverse distributions of mean temperature (**a**) and c'' (**b**) for the filtered DNS data and for LES22 at $x/\Lambda = 4.0$

In Fig. 12, the RMS fluctuations of the streamwise u'', transverse v'' and spanwise w'' velocities for LES22 and LES43 are shown. The LES22 using the FDSGS combustion model predicts the peak positions of the u'', v'' and w'' distributions and gives relatively good predictions of u'' although the LES43 significantly underestimates v'' and w''. The introduction of the SSRM model gives higher values of u'', v'' and w'' and therefore, slightly better predictions than that with the Smagorinsky model. This is because the SSRM model considers the backward scatter of the kinetic energy and adequatly determines the eddy viscosity.

The distributions of the mean temperature and c'' for LES22 are shown in Fig. 13. The change of the stress model does not much influence the mean temperature and c'' distributions. From these results in Figs. 11, 12 and 13, it is found that the LES with the SSRM model seems to be reasonable for the velocity fluctuations although the LES shows almost same predictions for the distributions of mean velocity, mean temperature and the progress variable fluctuations.

7 Conclusion

In this study, the FDSGS combustion model, the scalar flux models and the SSRM stress model are evaluated by conducting *a priori* and *a posteriori* tests with DNS data of the hydrogen-air turbulent jet premixed flame. *A priori* tests of the several scalar flux models reveal that the model proposed by Clark et al. [8] accurately predicts the counter-gradient transport as well as the gradient transport. From *a posteriori* tests of the combustion models, it is found that the LES using the FDSGS combustion model adequately predicts the mean temperature distributions and the peak positions of the transverse distributions of the filtered progress variable fluctuations. The model proposed by Chatakonda et al. [7] also shows good performances under the conditions of the present study. *A posteriori* tests of the scalar flux models show that the model of Clark et al. [8] gives better predictions for the filtered progress variable fluctuations than the gradient diffusion model although the changes of the results for the different scalar flux models are not as significant as those for the different combustion models. The evaluations of the stress models reveal that the LES with the SSRM model predicts the velocity fluctuations slightly better than that with the Smagorinsky model.

Acknowledgements This work is partially supported by Grant-in-Aid for Scientific Research (S) (No. 23226005) of Japan Society for the Promotion of Science.

References

1. Bardina, J., Ferziger, J., Reynolds, W.: Improved subgrid-scale models for large-eddy simulation. AIAA J. **80**(1357) (1980)
2. Baum, M., Poinsot, T., Thevenin, D.: Accurate boundary conditions for multicomponent reactive flows. J. Comput. Phys. **106**, 247–261 (1994)
3. Boger, M., Veynante, D., Boughanem, H., Trouvé, A.: Direct numerical simulation analysis of flame surface density concept for large eddy simulation of turbulent premixed combustion. Proc. Combust. Inst. **27**(1), 917–925 (1998)
4. Brown, P., Byrne, G., Hindmarsh, A.: VODE: A variable-coefficient ODE solver. SIAM J. Sci. Statist. Compt. **10**, 1038–1051 (1989)
5. Chakraborty, N., Klein, M.: A *priori* direct numerical simulation assessment of algebraic flame surface density models for turbulent premixed flames in the context of large eddy simulation. Phys. Fluids **20**(085), 108 (2008)
6. Charlette, F., Meneveau, C., Veynante, D.: A power-law flame wrinkling model for LES of premixed turbulent combustion part I: Non-dynamic formulation and initial tests. Combust. Flame **131**, 159–180 (2002)
7. Chatakonda, O., Hawkes, E.R., Brear, M.J., Chen, J.H., Knudsen, E., Pitsch, H.: Modeling of the wrinkling of premixed turbulent flames in the thin reaction zones regime for large eddy simulation. Proc. CTR Summer Program., 271–280 (2010)
8. Clark, R.A., Ferziger, J.H., Reynolds, W.C.: Evaluation of subgrid-scale models using an accurately simulated turbulent flow. J. Fluid Mech. **91**(1), 1–16 (1979)
9. Colin, O., Ducros, F., Veynante, D., Poinsot, T.: A thickened flame model for large eddy simulation of turbulent premixed combustion. Phys. Fluids **12**(7), 1843–1863 (2000)
10. Damköhler, G.: Der einfluss der turbulenz auf die flammengeschwindigkeit in gasgemischen. Z. Elektrochem. **46**(11), 601–626 (1940)
11. Domingo, P., Vervisch, L., Payet, S., Hauguel, R.: DNS of a premixed turbulent V flame and LES of a ducted flame using a FSD-PDF subgrid scale closure with FPI-tabulated chemistry. Combust. Flame **143**, 566–586 (2005)
12. Flohr, P., Pitsch, H.: A turbulent flame speed closure model for LES of industrial burner flows. Proc. CTR Summer Program., 169–179 (2000)
13. Fukushima, N., Naka, Y., Hiraoka, K., Shimura, M., Tanahashi, M., Miyauchi, T.: A scale self-recognition mixed SGS model based on the universal representation of Kolmogorov length by GS variables. In: Proc 9th Turbulence and Shear Flow Phenomena (2015)
14. Fureby, C.: A fractal flame-wrinkling large eddy simulation model for premixed turbulent combustion. Proc. Combust. Inst. **30**, 593–601 (2005)
15. Gao, Y., Chakraborty, N., Klein, M.: Assessment of the performances of sub-grid scalar flux models for premixed flames with different global lewis numbers: A direct numerical simulation analysis. Int. J. Heat Fluid Flow **52**, 28–39 (2015)
16. Germano, M., Piomelli, U., Moin, P., Cabot, W.H.: A dynamic subgrid-scale eddy viscosity model. Phys. Fluids **3**(7), 1760–1765 (1991)
17. Gicquel, L.Y.M., Staffelbach, G., Poinsot, T.: Large eddy simulation of gaseous flames in gas turbine combustion chambers. Prog. Energy Combust. Sci. **38**, 782–817 (2012)
18. Gutheil, E., Balakrishnan, G., Williams, F.A.: Structure and extinction of hydrogen–air diffusion flames. In: Peters, N., Rogg, B. (eds.) Lecture Notes in Physics: Reduced kinetic mechanisms for applications in combustion systems., pp. 177–195. Springer Verlag, New York (1993)
19. Haworth, D.C.: Progress in probability density function methods for turbulent reacting flows. Prog. Energy Combust. Sci. **36**, 168–259 (2010)
20. Hiraoka, K., Minamoto, Y., Shimura, M., Naka, Y., Fukushima, N., Tanahashi, M.: A fractal dynamic SGS combustion model for large eddy simulation of turbulent premixed flames. Comb. Sci. Technol.
21. Huai, Y., Sadiki, A., Pfadler, S., Löffler, M., Beyrau, F., Leipertz, A., Dinkelacker, F.: Experimental assessment of scalar flux models for large eddy simulations of non-reacting flows. Proc. 5th Turbulence. Heat Mass Transf., 263–266 (2006)
22. Jiang, G.S., Peng, D.: Weighted ENO schemes for Hamilton-Jacobi equations. SIAM J. Sci. Comput. **21**, 2126–2143 (2000)

23. Kerstein, A.R., Ashurst, W.T., Williams, F.A.: Field equation for interface propagation in an unsteady homogeneous flow field. Phys. Rev. A **37**(7), 2728–2731 (1988)
24. Kim, J., Pope, S.B.: Effects of combined dimension reduction and tabulation on the simulations of a turbulent premixed flame using a large-eddy simulation/probability density function method. Combust. Theory Model **18**(3), 388–413 (2014)
25. Knikker, R., Veynante, D., Meneveau, C.: A dynamic flame surface density model for large eddy simulation of turbulent premixed combustion. Phys. Fluids **16**(11), 91–94 (2004)
26. Kobayashi, H.: The subgrid-scale models based on coherent structures for rotating homogeneous turbulence and turbulent channel flow. Phys. Fluids **17**(045), 104 (2005)
27. Lele, S.K.: Compact finite difference schemes with spectral-like resolution. J. Comput. Phys. **103**, 16–42 (1992)
28. Lipatnikov, A.N., Chomiak, J.: Effects of premixed flames on turbulence and turbulent scalar transport. Prog. Energy Combust. Sci. **36**, 1–102 (2010)
29. Liu, X.D., Osher, S.: Chan., T.: Weighted essentially non-oscillatory schemes. J. Comput. Phys. **115**, 200–212 (1994)
30. Michalke, A.: On the inviscid instability of the hyperbolic-tangent velocity profile. J. Fluid Mech. **19**(4), 543–556 (1964)
31. Miyauchi, T., Tanahashi, M., Gao, F.: Fractal characteristics of turbulent diffusion flames. Comb. Sci. Technol. **96**, 135–154 (1994)
32. Nicoud, F., Ducros, F.: Subgrid-scale stress modelling based on the square of the velocity gradient tensor. Flow Turbulence Combust. **62**, 183–200 (1999)
33. Peters, N.: Turbulent Combustion. Cambridge Press (2000)
34. Pfadler, S., Kerl, J., Beyrau, F., Leipertz, A., Sadiki, A., Scheuerlein, J., Dinkelacker, F.: Direct evaluation of the subgrid scale scalar flux in turbulent premixed flames with conditioned dual-plane stereo PIV. Proc. Combust. Inst. **32**, 1723–1730 (2009)
35. Pitsch, H.: A consistent level set formulation for large-eddy simulation of premixed turbulent combustion. Combust. Flame **143**(4), 587–598 (2005)
36. Pitsch, H.: Large eddy simulation of turbulent combustion. Annu. Rev. Fluid Mech. **38**, 453–482 (2006)
37. Pitsch, H., Duchamp De Lageneste, L.: Large-eddy simulation of premixed turbulent combustion using a level-set approach. Proc. Combust. Inst. **29**, 2009–2015 (2002)
38. Poinsot, T.J., Lele, S.K.: Boundary conditions for direct simulations of compressible viscous flows. J. Comput. Phys. **101**, 104–129 (1992)
39. Richard, S., Colin, O., Vermorel, O., Benkenida, A., Angelberger, C., Veynante, D.: Towards large eddy simulation of combustion in spark ignition engines. Proc. Combust. Inst. **31**, 3059–3066 (2007)
40. Shim, Y., Tanaka, S., Tanahashi, M., Miyauchi, T.: Local structure and fractal characteristics of H_2-air turbulent premixed flame. Proc. Combust. Inst. **33**, 1455–1462 (2011)
41. Shimura, M., Yamawaki, K., Fukushima, N., Shim, Y.S., Nada, Y., Tanahashi, M., Miyauchi, T.: Flame and eddy structures in hydrogen-air turbulent jet premixed flame. J. Turbulence **13**(42), 1–17 (2012)
42. Tanahashi, M., Iwase, S., Miyauchi, T.: Appearance and alignment with strain rate of coherent fine scale eddies in turbulent mixing layer. J. Turbulence **2**(6), 1–18 (2001)
43. Thornber, B., Bilger, R.W., Masri, A.R., Hawkes, E.R.: An algorithm for LES of premixed compressible flows using the conditional moment closure model. J. Comput. Phys. **230**, 7687–7705 (2011)
44. Tullis, S., Cant, R.S.: Scalar transport modeling in large eddy simulation of turbulent premixed flames. Proc. Combust. Inst. **29**, 2097–2104 (2002)
45. Veynante, D., Trouvé, A., Bray, K.N.C., Mantel, T.: Gradient and counter-gradient scalar transport in turbulent premixed flames. J. Fluid Mech. **332**, 263–293 (1997)
46. Veynante, D., Vervisch, L.: Turbulent combustion modeling. Prog. Energy Combust. Sci. **28**, 193–266 (2002)
47. Weller, H.G., Tabor, G., Gosman, A.D., Fureby, C.: Application of a flame-wrinkling LES combustion model to a turbulent mixing layer. Proc. Combust. Inst. **27**, 899–907 (1998)
48. Yoshikawa, I., Shim, Y.S., Nada, Y., Tanahashi, M., Miyauchi, T.: A dynamic SGS combustion model based on fractal characteristics of turbulent premixed flames. Proc. Combust. Inst. **34**, 1373–1381 (2013)